4

CFD for Characterizing Standard and Single-use Stirred Cell Culture Bioreactors

Stephan C. Kaiser, Christian Löffelholz, Sören Werner and Dieter Eibl
Zurich University of Applied Sciences, School of Life Sciences and Facility Management
Switzerland

1. Introduction

Driven by global competition and rising cost pressure in the pharmaceutical industry, over the last ten years single-use bioreactors have been increasingly used for animal cell cultivations in screening experiments, seed inoculum and seed train productions as well as in small and medium scale production processes of proteins (in particular, antibodies and vaccines). In contrast to re-usable bioreactors made of glass or stainless steel, single-use bioreactors consist of a flexible or rigid cultivation vessel which has been gamma-sterilized and made ready for the purchaser to use. After harvest, the cultivation vessel is discarded, which results in a lower risk of cross-contamination, and eliminates the need for steam sterilization and cleaning [Eibl et al. (2010)].

Nowadays a multitude of single-use bioreactors are commercially available, which can be categorized according to the type of power input into static and dynamic systems. The latter can be further subdivided into hydraulically, pneumatically and mechanically driven bioreactors and their combinations, the so-called hybrid systems [Eibl et al. (2011)]. Mechanically driven single-use bioreactors represent the largest group and are mixed by either orbital-shaken, wave-induced or stirrer motion.

While wave-mixed bioreactors (e.g. from GE Healthcare, Sartorius Stedim Biotech, Applikon Biotechnology) were initially dominant, nowadays stirred bag systems (such as Hyclone® Single Use Bioreactor S.U.B., BIOSTAT® CultiBag STR, XDR™-DSTB animal) are more frequently used, mainly due to the broad experience already obtained with conventional stirred cell culture bioreactors [Eibl et al. (2011)]. The flexible cultivation bags are fixed and shaped by a temperature-controlled stainless steel container. This design is also used in the BIOSTAT® CultiBag STR from Sartorius Stedim Biotech, which is available at different scales from 50 to 1,000 L. The bag geometry, the impellers and the aeration system are designed in a similar way to Sartorius Stedim's re-usable stirred cell culture bioreactors to ensure comparability of single-use and classical processes, and thus facilitate integration of single-use bioreactor technologies into modern cultivation processes [De Wilde et al. (2009); Noack et al. (2011)].

Until summer 2009, stirred bag bioreactors were available only at working volumes exceeding 50 L for manufacturing and cost reasons. The introduction of the first single-use stirred bioreactors with a rigid cultivation vessel (Mobius® CellReady 3L bioreactor and CelliGen® BLU SUB) bridged the gap for stirred systems between laboratory and pilot scale

[Kaiser et al. (2010)]. With the recent development of the UniVessel® single-use, Sartorius Stedim Biotech have extended their portfolio of the BIOSTAT® product family at bench scale. This novel cell culture bioreactor comes as close as possible to the conventional UniVessel®, but differs slightly in geometry due to the manufacturing process. Furthermore, the positioning of installations, such as harvest tubes or probes, are customized in the re-usable bioreactor, but fixed in the single-use alternative.
Comparability of single-use and conventional cell culture bioreactors is essential for process development, especially when both systems have to be used side by side in hybrid solutions. A need for single-use bioreactors with design and set-up comparable to the re-usable alternative is therefore evident. Hence, the aim of this case study is a comparison of the UniVessel® 2L single-use bioreactor with its conventional counterpart made out of glass (in the following, also referred to as 'small scale'). For this purpose, fluid flow investigations using computational fluid dynamics (CFD) are carried out for the single-use and conventional bioreactor to show that the small changes in the geometry of the single-use UniVessel® have no significant effect on its fluid flow. The commercial CFD software package ANSYS Fluent (version 12.1.3) is applied and engineering parameters, such as power input, mixing time and oxygen mass transfer, are determined for the first time. With regard to scale-up, the results are compared with those of the disposable BIOSTAT® CultiBag STR at 50 L scale (in the following, also referred to as 'large scale').

2. Issues related to scale-up in stirred cell cultures

For biomanufacturing processes requiring larger volumes, scalability of the bioreactor system is a crucial factor, because similar process characteristics have to be guaranteed over the different scales [Storhas (2003)]. The conventional scale-up of bioprocesses is based on physicochemical and geometrical similarity [Zlokarnik (2006)]. However, keeping one process parameter constant will change several others. Hence, the key parameters with the strongest influence on cell growth and productivity have to be identified. In aerobic cultivations, these are primarily oxygen mass transfer and carbon dioxide removal, mechanical stress and mixing intensity. According to Storhas (2006), all these parameters are influenced by the specific power input (power input per volume of culture broth), even though in different proportions (see Fig. 1). For example, mixing time in fully turbulent flows is proportional to the third radical of the specific power input (Eq. 1), resulting in longer mixing times at larger scales.

$$\theta_m \propto \left(P/V\right)^{-1/3} \tag{1}$$

In contrast, the highest local energy input ε_{max}, which is often related to mechanical stress, is proportional to the specific power input:

$$\varepsilon_{max} \propto \frac{u_{tip}^{\ 3}}{d} \propto P/V \tag{2}$$

Besides the specific power input, impeller tip speed u_{tip}, impeller Reynolds number Re, mixing time θ_m, oxygen mass transfer coefficient k_La and the Kolmogorov eddy length l_e are applied as scale-up/down criteria in biotechnology. However, the difficulty in the scale-up of cell culture processes results from a lack of preservation of local flow structures as the

reactor vessels are scaled-up [Venkat & Chalmers (1996)]. It is well-known that highly localized regions of high energy dissipation exist and that local flow structures greatly depend on the geometry and operation conditions of the vessels, and cannot be described adequately by global scale-up parameters. Therefore, spatial resolved data obtained by experimental [Venkat & Chalmers (1996)] and numerical techniques are increasingly being introduced in scale-up studies [Letellier et al. (2002)].

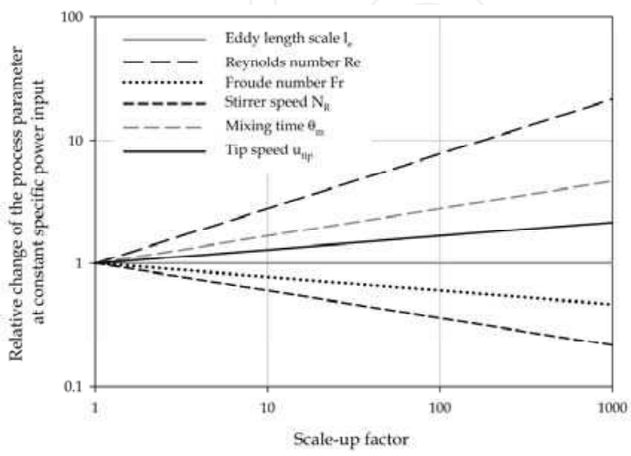

Fig. 1. Influence of scale on different process parameters at constant P/V

As previously mentioned, oxygen mass transfer is another important parameter for scale-up. Due to its low solubility in aqueous media, oxygen has to be continuously supplied to the culture. Animal cells have lower metabolic rates and oxygen demands compared with yeast and bacteria, but in high cell density processes or in cases where aeration is limited by mechanical stress tolerance, oxygen mass transfer can become a limiting factor [Ozturk (1996)]. Although some other options for oxygen supply are available, the use of sparging systems (e.g. ring sparger or microsparger) remains the most practicable method, especially at large scale [Arathoon & Birch (1986); Chisti (1993); Chalmers (1994)]. However, various reports of bubble-associated cell damage can be found in the literature [Handa et al. (1987); Oh et al. (1992); Kioukia et al. (1996)]. Because most agitated bioreactors used in cell culture operate at relatively low mechanical power input, mechanical stress caused by bubbles can exceed that of agitation. Bubble rupture at the liquid surface was found to have the highest effect due to the high local energy density occurring when bubbles burst [Jöbses et al. (1991); Chisti (2000)].

Cell cultures respond to external stresses by changes in morphology, proliferation, differentiation, metabolism or even cell death [Weyand et al. (2009)]. Nevertheless, the biological effects of mechanical stress also depend on culture broth properties (viscosity, oxygen saturation, metabolite concentration, additives, etc.) and can significantly differ between the cell types, cell lines and their characteristics (such as origin, age, subcultivation number etc.) [Meneses-Acosta et al. (2001); Krampe & Al-Rubeai (2010)]. Due to the complexity of the cell damage mechanisms and the variety of factors described in literature, it is still difficult to draw any general conclusions. However, it is accepted that minimum levels of energy dissipation are desirable for scale-up in order to provide sufficient mixing and avoid sedimentation, oxygen depletion and inhomogeneities [Venkat & Chalmers (1996)].

3. Numerical methodology

3.1 Description of bioreactors

In this study, the fluid flow patterns in stirred cell culture bioreactors at two different scales (2 L and 50 L) were investigated. The small scale bioreactors from the Sartorius Stedim Biotech's product family BIOSTAT® with the vessels UniVessel® 2L (made of glass) and its single-use counterpart, (UniVessel® 2L SU), have nearly identical geometries (see Tab. 1). Both systems have a cylindrical vessel with a dished bottom and are agitated by a combination of a Rushton turbine (RT) and a three-blade segment impeller (SBI), which are 53 mm and 55 mm in diameter respectively. Due to the manufacturing process, the diameter of the plastic vessel broadens towards the top (from 118 to 126 mm), its bottom has a different shape, and the diameter of the stirrer shaft is larger (at 15.2 mm). Furthermore, the positioning of installations, such as harvest tubes or probes, are fixed in the single-use alternative but customized in the re-usable bioreactor. For the CFD simulation of the glass vessel, the probes were designed based on the bioreactors which are used in our laboratory (see Fig. 2d).

	Symbol	BIOSTAT® CultiBag STR 50 L	UniVessel® 2L single-use	UniVessel® 2L re-usable
Filling height	H	490	180	165
Vessel diameter	D	370	118 – 126[1)]	130
Stirrer diameter				
RT	d_1	143	53	53
SBI	d_2	143	55	55
Stirrer height				
RT	w_1	27	10.5	10.5
SBI	w_2	68.6	30.4	30.4
Off-bottom clearance (distance from the bottom to the mid-plane of the lower impeller)	h	89.5	48.5	48.5
Clearance between stirrers (distance between the mid-planes of the impellers)	c	186	70	70
Shaft diameter	s	20	15.2	10

Table 1. Geometrical dimensions of the bioreactors investigated. All values are given in millimetres and the symbols are indicated in Fig. 2a. [1)] The single-use UniVessel® features a slight inclination of 1° due to the manufacturing process as compared to the re-usable vessel. Hence, the range of the vessel diameters is given. The mean value of 122 mm was used in calculations

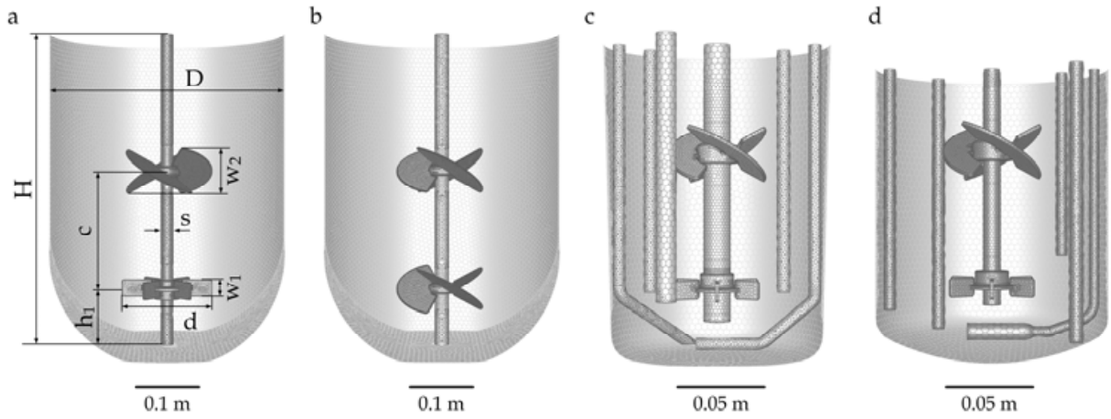

Fig. 2. CAD-models of the four bioreactors used in this study: BIOSTAT® CultiBag STR 50 L with two stirrer configurations (a) and (b), and the UniVessel® 2L single-use (c) with its conventional counterpart (d)

The geometry of the BIOSTAT CultiBag STR 50 L differs from the smaller scales primarily in its differently-shaped bottom (see Figs. 2a and 2b). Other parameters (e.g. d/D, H/D, c/D etc.) are geometrically similar. Inside the bag, no baffles are integrated and inside the vessel no additional elements, such as probes, are present because measurements of the pH value and oxygen concentration are realized by small optical sensors installed at the bottom of the bag near the wall. Their influence on the fluid flow is negligible.

3.2 Model equations and numerical details

The CFD investigations were realized using a RANS approach with the commercial software package Fluent (ANSYS, Inc. (version 12.1.3)). Using the pre-processor GAMBIT (version 2.4) the accurate bioreactor geometries, shown in Fig. 2, were discretized by body-fitted unstructured meshes. The tetrahedral control volumes were subsequently transformed to polyhedral cells as they have advantages of both tetrahedral and hexahedral cells [Paschedag et al. (2007)]. Prior to the investigations, the grid sensitivity of the CFD results was tested, indicating that meshes with about 130,000 cells for the UniVessel® and 180,000 cells for the BIOSTAT® CultiBag 50L are good compromises between acceptable calculation time and accuracy for further studies.

The governing equation for mass and momentum for single-phase flows can be written as:

$$\frac{\partial \rho}{\partial t} + \nabla \cdot \left(\rho \cdot \vec{u} \right) = 0 \tag{3}$$

$$\frac{\partial \left(\rho \cdot \vec{u} \right)}{\partial t} + \nabla \cdot \left(\rho \cdot \vec{u} \cdot \vec{u} \right) = -\nabla p + \nabla \cdot \bar{\bar{\tau}} + \rho \cdot \vec{g} + \vec{F} \tag{4}$$

where ρ is the fluid viscosity, $\vec{u}$ is the velocity vector, p is the static pressure, and the terms $\rho \cdot \vec{g}$ and $\vec{F}$ denote the gravitational and external body forces respectively. The Reynolds stress tensor $\bar{\bar{\tau}}$ was described by the standard k-ε turbulence model [Fluent (2006)].

For multi-phase simulations, an Euler-Euler approach was applied, which considers water as continuous and air as the dispersed phase. The mass and momentum conservation equations for the kth phase are given as:

$$\frac{\partial(\alpha_k \cdot \rho_k)}{\partial t} + \nabla \cdot (\alpha_k \cdot \rho_k \cdot \vec{u}_k) = 0 \tag{5}$$

$$\frac{\partial(\alpha_k \cdot \rho_k \cdot \vec{u}_k)}{\partial t} + \nabla \cdot (\alpha_k \cdot \rho_k \cdot \vec{u}_k \cdot \vec{u}_k) = \nabla \cdot \tau_{eff,k} - \alpha_k \cdot \nabla p + \alpha_k \cdot \rho_k \cdot \vec{g} + \vec{F}_k + \vec{R}_k \tag{6}$$

where $\vec{u}_k$ is the phase velocity vector (k = L the liquid phase and k = G the gas phase), ρ_k the phase density and α_k the phase volume fraction. A multi-phase k-ε turbulence model provided by Fluent was used with default settings [Fluent (2006)]. The drag force was modelled by a standard drag model with a correlation for the drag coefficient given by Ishii & Zuber (1979).

In both single- and multi-phase simulations, the vessel walls, the impeller and the probes were treated as non-slip boundaries with standard wall functions. Stirrer rotation was implemented using the Multiple Reference Frame model (MRF) in steady state simulations, which is a good compromise between physical accuracy and reasonable computational time. All equations were discretized using the First Order Upwind scheme, and the (phase-coupled) SIMPLE algorithm was chosen for pressure-velocity coupling. Convergence was assumed when the residuals decreased below 10^{-5}.

For the simulation of mixing process, the flow field obtained was used for a transient calculation of the concentration distribution of an inert tracer superimposed on the flow field. Assuming tracer distribution by convection and diffusion, the species transport equation is given by:

$$\frac{\partial(\rho \cdot \beta)}{\partial t} + \nabla \cdot (\rho \cdot \vec{u} \cdot \beta) = -\nabla \cdot (\rho \cdot D_{eff} \cdot \nabla \beta) \tag{7}$$

where β is the mass fraction of the tracer and D_{eff} is the effective diffusion coefficient, which is calculated using the following equation [Fluent (2006)]:

$$D_{eff} = D_m + \frac{\eta_t}{Sc_t} \tag{8}$$

where D_m, η_t and Sc_t represent the molecular diffusion coefficient, the turbulent viscosity and the turbulent Schmidt number (which is 0.7 by default) respectively. The tracer was injected at the liquid surface (at r/R = 0.5) and the concentration was monitored at eight different points inside the bioreactor. The mixing time was defined as the time required to achieve 95% homogeneity defined by Eq. 9, where β_∞ is the mass fraction in its equilibrium value.

$$H(t) = \frac{|\beta(t) - \beta_\infty|}{\beta_\infty} \tag{9}$$

4. Results and discussion

4.1 Single-phase flow pattern

As described above, animal cell cultures are sensitive to shear stress, which is often related to the impeller tip speed. Although there are some doubts from the fluid dynamic perspective, maximum tolerable tip speeds are described in the literature [Fenge, et al. (1993); Varley & Birch (1999)]. Maximum tolerable tip speeds differ between cell lines: hybridoma cells were found to tolerate the highest values of up to 1.8 $m \cdot s^{-1}$ [Chisti (2001)]. Hence, the flow fields in this study were simulated for various rotational speeds up to 625 rpm (corresponding to u_{tip} = 1.8 $m \cdot s^{-1}$) in the UniVessel® system. The tip speeds were subsequently adopted for the simulations of the 50 L scale BIOSTAT® CultiBag STR.

In the following sections, the predicted single-phase fluid flow patterns are described and compared in respect of the two small scale bioreactors. Important engineering characteristics, such as power input and mixing time, are subsequently described. Furthermore, attempts to predict mechanical stress on the cells are presented.

The CFD-predicted fluid flow pattern for the two small scale cell culture bioreactors under unaerated conditions are given in Fig. 3. In both vessels, the upper segment blade impeller (SBI) shows a clear axial flow profile in down-pumping mode while the lower Rushton turbine (RT) discharges the fluid radially towards the vessel wall. The fluid impinges on the outer wall, splits and moves upwards and downwards forming two recirculation loops per half-vessel. In the lower loop, the highest velocities in the order of $0.5 \cdot u_{tip}$ are observed in the vicinity of the RT, dropping to $0.1 \cdot u_{tip}$ near the vessel bottom. In the vicinity of the upper impeller, fluid velocities reach about $0.4 \cdot u_{tip}$, but are significantly lower near the liquid surface.

As described by Alcamo et al. (2005), the jet of the RT has a slight downward inclination, which can be explained by the absence of baffles. In contrast, slight upwardly inclined radial jets have been found in experimental [Yianneskis et al. (1987)] and numerical [Montante et al. (2001)] studies on fully baffled vessels with Rushton turbines. An interaction of the two impellers can be neglected due to the distance between their mid-plains of $c/d \approx 1.25$ [Liepe et al. (1998); Vrabel et al. (2000)], which is also confirmed by the estimated power input (see Section 4.2.1).

A more quantitative analysis of the velocity field is presented in Figs. 4 and 5, which show normalised radial, tangential and axial fluid velocities at different positions inside the vessel. In each case, nearly identical fluid velocities are obtained in the UniVessel® single-use and its glass counterpart. The small remaining differences can be ascribed to numerical errors and the fact that the meshes are almost, but not completely, identical.

The maximum radial velocity in the RT's discharge is located below the mid-impeller plain, resulting in an asymmetric profile (see Fig. 4a). Compared with data given by Alcamo et al. (2005) for a single Rushton turbine in an unbaffled vessel, qualitative agreement is achieved, although higher values of radial velocity of up to $0.4 \cdot u_{tip}$ are obtained in this study. This might be an effect of the indirect baffling caused by the probes used in this study since the radial velocities obtained for the completely unbaffled BIOSTAT® CultiBag 50L are more similar to data given in the literature [Alcamo et al (2005)]. In contrast, Delafosse et al. (2008) and Kresta & Wood (1991) give maximum radial velocities in the stirrer discharge of up to $0.8 \cdot u_{tip}$.

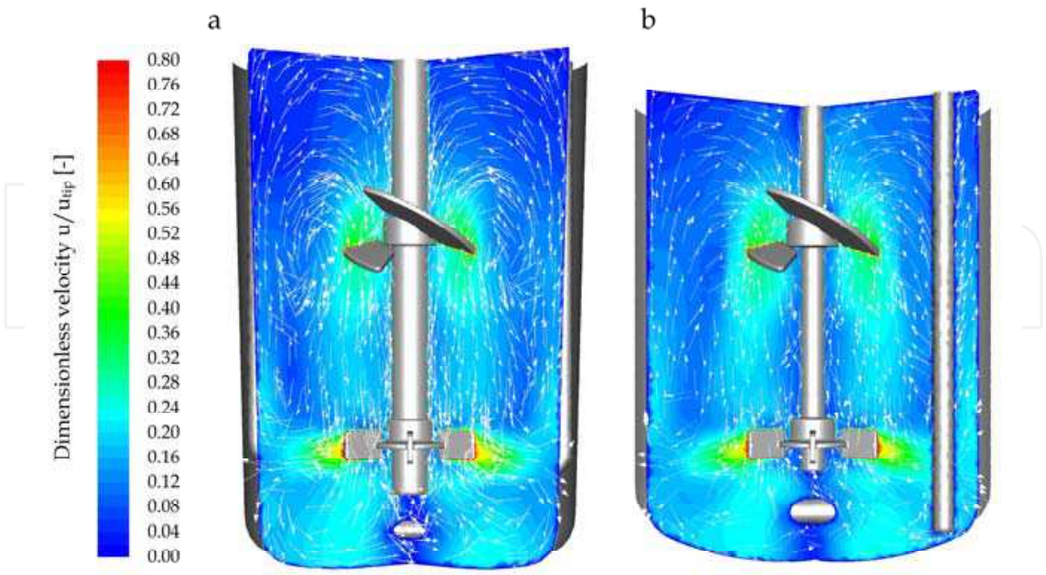

Fig. 3. Velocity distribution in the two small scale vessels UniVessel® single-use (a) and UniVessel® re-usable (b) represented by dimensionless velocity u/u_{tip}. The velocity magnitude is indicated by contour plots. The velocity vectors are projected to the given plains with fixed length

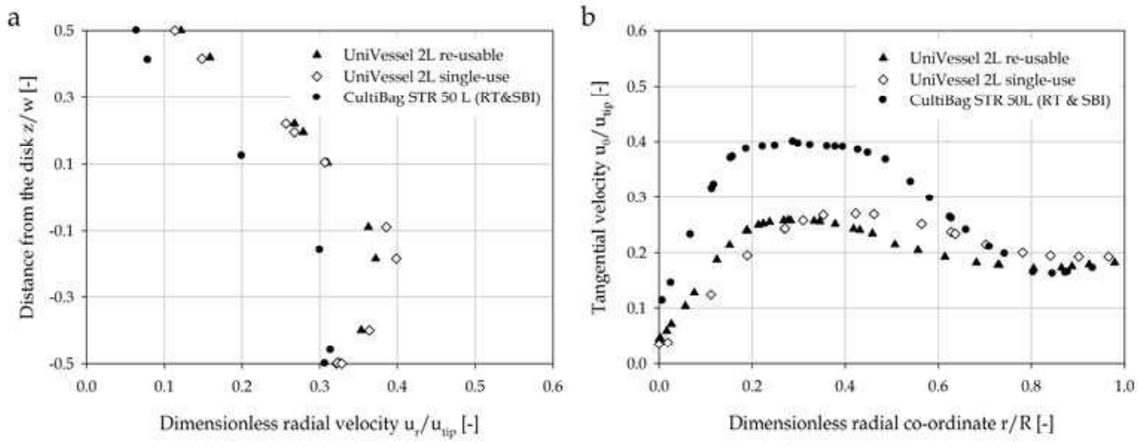

Fig. 4. Comparison of dimensionless radial (a) and tangential velocities (b) between the bioreactors investigated. The radial velocities are given at a distance of 2r/d = 0.57 from the impeller tip and the tangential velocities are shown for z/D = 0.2

Similar results are found for tangential velocity, where good agreements between the two small scale vessels are again found. The maximum tangential velocity of $0.3 \cdot u_{tip}$ is predicted near r/R = 0.4, which is qualitatively comparable to the findings of Alcamo et al. (2005). Due to the higher radial component found in this study, the tangential velocity is lower than those reported, whereas the values for the 50 L scale vessel are more comparable to those described in literature [Alcamo et al (2005)].

In Fig. 5, radial profiles of the axial velocities directly above and below the upper impeller are shown. The maximum axial velocities in the impeller's discharge are located at r/R = 0.4 in both cases and have values of $u_z \approx 0.2 \cdot u_{tip}$. Zhu et al. (2009) give PIV data of an axial pumping "elephant ear" impeller (Applikon Biotechnology) in an unbaffled vessel with similar geometries to that of the SBI. Good qualitative agreement is obtained between PIV measurements and our CFD results. The recirculation points, where up- and down-flow meet and axial velocities become zero, are nearly identical between the two impellers. However, the maximum velocities determined in the impeller's discharge and near the vessel wall have lower values for the segment impeller with $u_z = 0.2 \cdot u_{tip}$ and $u_z = 0.05 \cdot u_{tip}$ respectively (see Fig. 5a). If the axial velocities of the small scale vessels are compared with the 50 L scale, good quantitative agreement is evident below the impeller, but some differences occur above the SBI. Thus, maximum velocity in the discharge of the larger impeller is shifted to the left (to r/R = 0.1) and lower values of $u_z \approx 0.02 \cdot u_{tip}$ are found near the wall (see Fig. 5b).

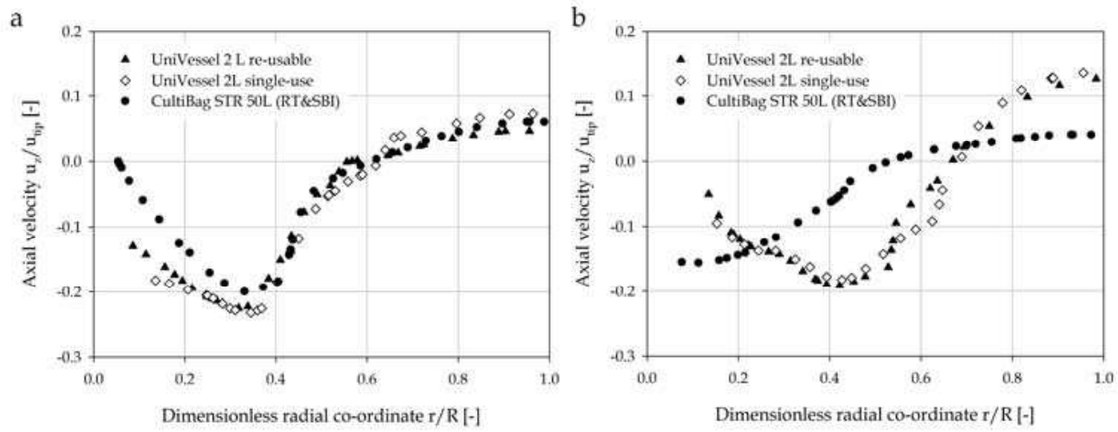

Fig. 5. Dimensionless axial velocities u_z/u_{tip} as a function of the radial co-ordinate below (a) and above (b) the upper impeller (with $\Delta z/d = 0.27$)

For further comparison, the dimensionless axial and radial circulation or pumping numbers Fl_z and Fl_r of the two impellers were calculated using the predicted flow field. Primary and secondary pumping numbers $Fl_{z,p}$ and $Fl_{z,s}$ as defined by Patwardhan et al. (1999) were calculated for the axial impeller using Eqs. 10 and 11. Both integrals were evaluated closest to the impeller in the pumping direction, whereas the axial flow was integrated over the impeller radius and to the point of reversal of the flow ($r = R_r$).

$$Fl_{z,p} = \frac{2\pi}{N \cdot d^3} \int_{r=0}^{r=d/2} r \cdot v_z(r)\, dr \tag{10}$$

$$Fl_{z,p} = \frac{2\pi}{N \cdot d^3} \int_{r=0}^{r=R_r} r \cdot v_z(r)\, dr \tag{11}$$

$$Fl_r = \frac{2\pi}{N \cdot d^3} \int_{z_1}^{z_2} r \cdot v_r(z)\, dz \tag{12}$$

In doing so, radial flow numbers for the Rushton turbine of 0.56 and 0.36 are determined in the small and large scale vessels respectively. Again no differences are found between the

plastic and the glass bioreactor. However, as a result of the downward inclined stirrer jet investigated in this study, both values are lower than 0.71, as the value reported for fully baffled tanks by Revstedt et al. (1998). The primary and secondary axial flow numbers for the small scale vessel are found to be 0.4 and 0.77. Zhu et al. (2009) obtained a primary flow number of 0.7 for the "elephant ear" impeller and Liepe et al. (1998) reported values for the secondary flow number between 0.7 and 2.2 for different axial pumping stirrers. The latter indicate that the pumping capacity could be increased by about 30 % when baffling is used.

4.2 Engineering characteristics and scale-up issues

4.2.1 Power input

Using the predicted flow, the impellers' power inputs were obtained from the torque acting on the stirrer and the shaft. The dimensionless power number (also called Newton number) was calculated as:

$$Ne = \frac{P}{\rho \cdot N^3 \cdot d^5} = \frac{2\pi \cdot M_R}{\rho \cdot N^2 \cdot d^5} \tag{13}$$

In Fig. 6a, the determined power numbers are given as a function of the impeller Reynolds number. Decreasing values for Ne are obtained in all investigated cases up to critical Reynolds numbers of $Re_{crit} \approx 10^4$, which is most often found in typical agitated systems [Zlokarnik (1999)]. Above the critical Reynolds number, the stirrer torque is not fully compensated by wall shear stresses and the power number becomes constant [Liepe et al. (1998)]. The CFD simulations resulted in values for the power number of 3.33 and 3.14 in the bioreactors agitated by RT and SBI at small and large scale respectively. As already indicated by the flow field, the probes seem to have a small effect on the power input. For the configuration with two SBIs the Newton number is lower at a value of 1.13. It is well-known that impellers in unbaffled vessels show a continuous decrease in the Newton number over a range of $0 < Re <\approx 5 \cdot 10^5$ due to vortex formation [Liepe et al. (1998)]. However, this effect was not taken into account in this study and the predicted values are in good agreement with experimental data provided by Sartorius Stedim Biotech. These were obtained by torque measurements and revealed power numbers of 3.4 with RT and SBI, and 1.2 with two SBIs [Personal communication, Ute Noack, Sartorius Stedim Biotech, 2010].

In Fig. 6b, the specific power input is shown as a function of the tip speed. For the maximum tip speed investigated in this study (1.8 $m \cdot s^{-1}$), the highest specific power input at 50 L scale is 240 $W \cdot m^{-3}$. The configuration with the two SBIs reaches only 86 $W \cdot m^{-3}$ due to the lower power number. Typical values of specific power input are about 100 $W \cdot m^{-3}$ [Henzler & Kauling (1993)], although Nienow (2006) gives a range of 10 to 250 $W \cdot m^{-3}$. However, if the impeller tip speed is used as a scale-up/down criterion, the power input at small scale increases significantly, as the relationship in Eq. 14 confirms:

$$P/V \propto \frac{u_{tip}}{d} \tag{14}$$

Thus, at a tip speed of 1.8 $m \cdot s^{-1}$ the specific power input increases up to 960 $W \cdot m^{-3}$ in the small scale bioreactors investigated, which is unreasonably high for cell culture applications. On the other hand, if the tip speed for moderate power input in small scale systems (e.g. 0.37 $m \cdot s^{-1}$ for about 10 $W \cdot m^{-3}$) is adopted in the larger scale CultiBag STR 50L, the P/V drops significantly (to about 1 $W \cdot m^{-3}$). Thus, maintaining tip speed at such low values is a major

constraint with severe implications for mass transfer as well as homogeneity (see Section 4.2.2). Although impeller tip speed is often used for scaling-up in the pharmaceutical industry, these results emphasize that the tip speed does not appear to be an important parameter for scale-up, which aligns with the findings of Nienow (2006).

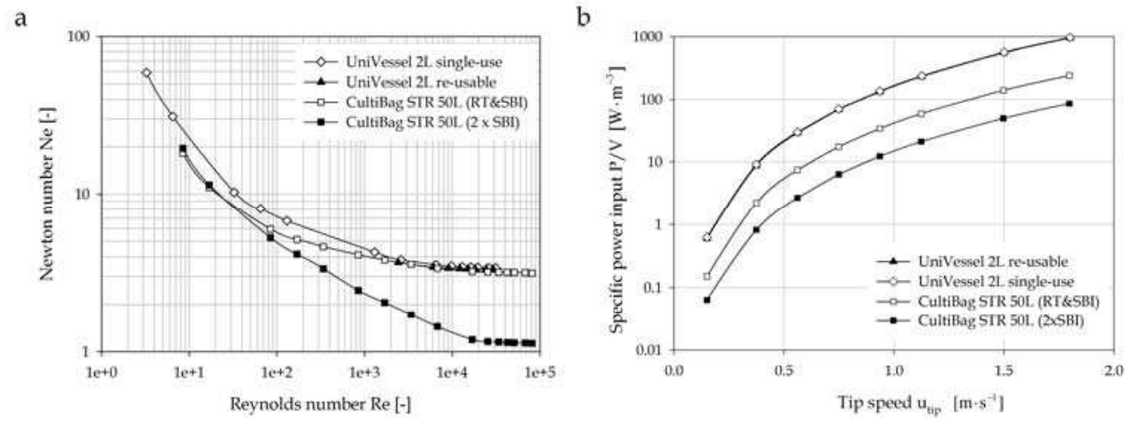

Fig. 6. Power characteristics of the four bioreactor configurations investigated (a). Specific power input as a function of tip speed (b). Note that the symbols for the UniVessel® 2L single-use are partly hidden by those of the UniVessel® re-usable

4.2.2 Mixing time

Mixing time was determined by addition of an inert tracer based on predicted flow field. The volume of the added tracer was equal to 0.1 % of the vessel content in all cases investigated. Typical tracer response curves for different tip speeds at a point near the upper impeller in the UniVessel® 2L single-use are given in Fig. 7. As reported by Min & Gao (2006) and Jahoda et al. (2007), the RANS approach with standard k-ε turbulence model fails to predict reasonable tracer response curves due to the under-prediction of turbulent fluctuations. However, good agreement of the mixing time with experimental results is usually obtained, as previously found in several studies in our laboratory on different glass and single-use bioreactors [Kaiser (2009); Löffelholz et al. (2011)].

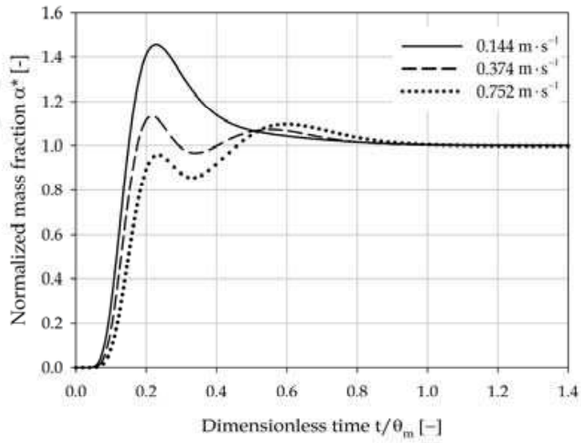

Fig. 7. Tracer response curve for different tip speeds at a point near the upper stirrer in the UniVessel 2L single-use. For better comparison, time is given as dimensionless

In Fig. 8, mixing times for all cases investigated are shown as a function of the specific power input (P/V). For the small scale systems, mixing times between 2.3 and 7.4 s are predicted, depending on the stirrer speed. As expected, only minor variations are again observed between the single-use and re-usable vessel types, which can be attributed to the different liquid heights present for equal volumes. In the BIOSTAT® CultiBag STR 50L, mixing times between 10 and 59.8 s are required to achieve the homogeneity desired, whereas the two segment impellers show significantly lower mixing times compared with the configuration of the RT and the SBI at a certain specific power input. The reason for this is the lower power number of the SBI, which results in higher stirrer speeds being required to achieve a certain power input. The stirrer speed is directly related to turbulence intensity, which improves mixing [Liepe et al. (1998); Kraume (2003)]. The slopes of the regression functions (see Fig. 8a) are between -0.36 and -0.3, and are close to the theoretical value of -0.33 (see Eq. 1), which is valid for turbulent conditions where

$$c_H = \theta_m \cdot N_R = \text{const.} \tag{15}$$

The mixing numbers calculated, which represent the stirrer rotations required to achieve the homogeneity desired, are 18 and 35 for the small and large scale bioreactors respectively. These values indicate that the agitation of the Sartorius Stedim's bioreactors is in the performance range of conventional impellers, as reported by Liepe et al. (1998).

Based on turbulence theory, it was suggested that mixing time is independent of impeller type and inversely proportional to turbulent diffusion so that:

$$\theta_m \propto \left(\frac{\varepsilon_T}{L_c^{\,2}} \right)^{-1/3} \tag{16}$$

where ε_T is the local energy dissipation rate and L_c is the integral scale of turbulence. Assuming that the integral scale is proportional to the vessel diameter, Nienow (1997) gives a correlation for mixing time with the third radical of the specific power input and geometrical parameters:

$$\theta_m = A \cdot \left(\frac{P}{V} \right)^{-1/3} \cdot \left(\frac{d}{D} \right)^{-1/3} \cdot \left(\frac{H}{d} \right)^{2.43} \cdot D^{2/3} \tag{17}$$

in which the term $(H/d)^{2.43}$ was originally developed for multiple impellers but also indicates the influence of the fill height observed in large-scale animal cell culture bioreactors at an aspect ratio of 1.3 with a single impeller working in draw and fill mode [Nienow (2006)].

If this approach is adapted to the CFD-predicted mixing times, two distinct functions are obtained for the reactor mixed by the RT/SBI combination and for the two axial pumping stirrers. Thus, the proportionality factor A in Eq. 17 is found to be 6.5 and 8.7 in the two functions respectively. They are in the same order of magnitude to the value of 5.9 found by Nienow (1997). Although mixing time is not an appropriate parameter for scale-up (see Section 2), homogeneity becomes increasingly important with respect to pH and nutrients at larger scales, and thus mixing capacity should be taken into account.

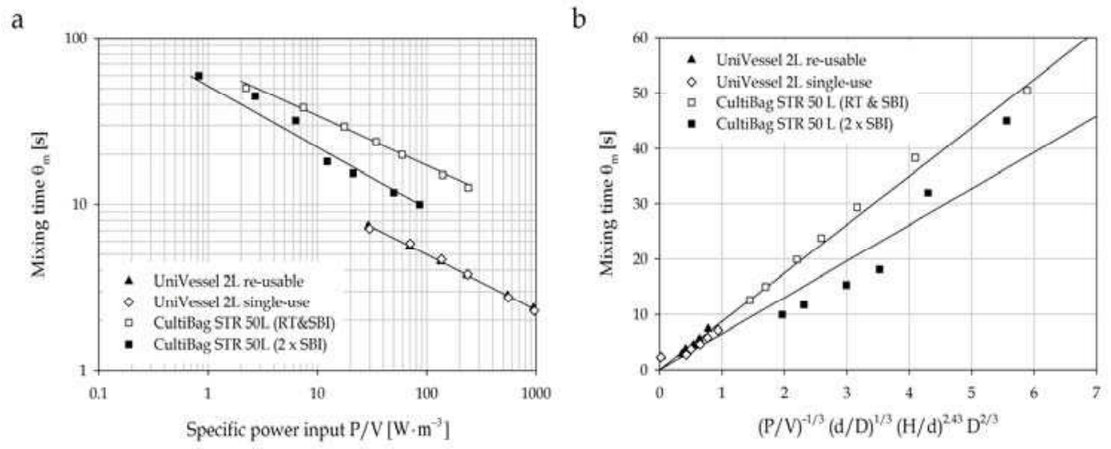

Fig. 8. Mixing time as a function of specific power input for all bioreactor configurations investigated (a). Comparison of the CFD-predicted mixing times with the correlation by Eq. 17 for all bioreactor configurations investigated (b)

4.2.3 Gas distribution and oxygen mass transfer

The gas phase distribution was modelled using an Euler-Euler approach, assuming a uniform bubble size with a diameter of 1 mm. This value was found to be the mean bubble size, determined by photography in the re-usable UniVessel® filled with pure water (2 L filling volume). Spatial gas phase distribution and oxygen mass transfer were investigated for different stirrer tip speeds in the range of 0.15 to 1.8 m·s^{-1} for two aeration rates of 0.1 and 0.2 vvm (volume gas per volume liquid and minute), which were defined via gas inlet velocity with gas volume fractions at the inlet surface equal to one.

Due to the low gassing rate, as often used in cell culture applications, no profound effect on the shape of the flow pattern is found, which is in qualitative agreement with the findings of Zhu et al. (2009). Small effects on the liquid velocity are predicted in the jet of the radial impeller, which becomes less intensive, as well as near the stirrer shaft, where the rising gas partly compensates for the downwards directed fluid flow (data not shown).

In Fig. 9, the spatial gas phase distribution is given for impeller tip speeds of 0.37 m·s^{-1} and 0.94 m·s^{-1} at an aeration rate of 0.1 vvm and compared with experimental observations of the re-usable UniVessel®. Good qualitative agreement is achieved for all operation conditions investigated. At low agitation, the greater part of the gas rises with low dispersion as the disruptive forces induced by the RT are insufficient to overcome buoyancy, although the RT is designed and commonly used to achieve homogeneous gas-liquid dispersions. However, at such low agitation, the stirrer is considered to be "flooded" [Liepe et al. (1998); Zlokarnik (1999)]. The gas dispersion is clearly enhanced by the higher stirrer speed, as shown in Figs. 9c and 9d. Under such conditions, the air introduced is dispersed radially by the lower stirrer and reaches the vessel wall, but almost no gas is found near the bottom. This is again in qualitative agreement with experimental observations (see Fig. 9c) and is also found in experimental [Zhu et al. (2009)] and numerical investigations [Kerdouss et al. (2008] at comparable operation conditions in other gas-liquid agitated vessels.

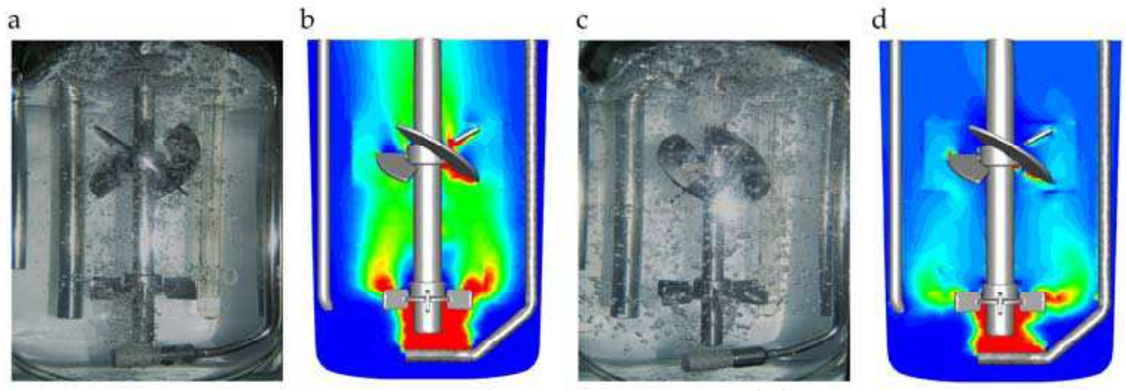

Fig. 9. Comparison of experimental observed gas distribution in the re-usable UniVessel® and CFD-predicted results for the single-use vessel at impeller tip speeds 0.37 m·s^{-1} (a) and 0.94 m·s^{-1} (b)

Based on the predicted flow field, specific oxygen mass transfer coefficients k_La were calculated as the product of the liquid mass transfer coefficient k_L and the specific surface area a, as suggested by Dhanasekharan et al. (2005) and Kerdouss et al. (2008). Assuming spherical bubble shape, which is guaranteed up to a bubble diameter of 3 mm [Gimbun et al. (2009)], the specific surface area is calculated by:

$$a = \frac{6 \cdot \alpha_G}{d_B} \tag{18}$$

The liquid transfer coefficient is obtained based on Higbie's penetration theory as shown in Eq. 19, where D_{O_2} represents the diffusion coefficient ($2.01 \cdot 10^{-9}$ m^2·s^{-1} at 20 °C).

$$k_L = \frac{2}{\sqrt{\pi}} \cdot \sqrt{D_{O_2}} \cdot \left(\frac{\varepsilon_L \cdot \rho_L}{\eta_L} \right)^{1/4} \tag{19}$$

The results of these calculations are summarized in Tab. 2. It is evident that oxygen mass transfer is enhanced by high agitation and aeration rates, as has been shown on numerous occasions for various stirrer systems. Higher stirrer speed (i.e. higher specific power input) results in lower oxygen transfer resistance due to the higher surface renewal rate of the bubbles [Gimbun et al. (2009)], which is represented by higher k_L values. Here, values between 3.15 and $5.95 \cdot 10^{-4}$ m·s^{-1} are predicted, which are almost independent of the aeration rate. In contrast, significantly higher air volume fractions are obtained for the higher aeration rate, as expected. Interestingly, a maximum overall gas hold-up of about 0.37 % and 0.66 % is reached at 30 W·m^{-3} for each aeration rate respectively, which is not enhanced by more rigorous agitation.

The highest k_La value, 96.3 h^{-1}, is obtained at 0.2 vvm and 625 rpm (see also Fig. 10a). This value is more typical of microbial fermentations, where higher oxygen demands have to be met. However, these high values are not entirely unexpected since the specific power input is also very high (see discussion in Section 4.2.1). Typical values for cell culture applications are in the range of 1 to 15 h^{-1} [Henzler & Kauling (1993); Langheinrich et al. (2002); Nienow (2006)].

Q [vvm]	P/V [W·m^{-3}]	k_L [10^{-4} m·s^{-1}]	a [m^2·m^{-3}]	α [%]	k_La [h^{-1}]
0.1	0.6	3.15	14.0	0.23	18.7
0.1	9.1	3.06	18.8	0.31	25.7
0.1	30.0	3.25	21.9	0.37	31.5
0.1	136.6	4.07	19.1	0.32	34.2
0.1	558.6	5.32	18.9	0.32	44.4
0.1	962.6	5.95	19.3	0.32	51.0
0.2	0.6	3.16	22.5	0.38	32.5
0.2	9.1	3.09	32.5	0.54	45.0
0.2	30.0	3.23	39.6	0.66	56.4
0.2	136.6	4.02	37.5	0.63	64.9
0.2	558.6	5.26	37.1	0.62	84.1
0.2	962.6	5.90	38.0	0.63	96.3

Table 2. Summary of the results of the multi-phase simulations in the UniVessel® single-use. The symbols Q, P/V, k_L, a, α and k_La represent the aeration rate, the specific power input, the liquid oxygen mass transfer coefficient, the specific surface area, and the overall oxygen mass transfer coefficient

To meet the oxygen demand of cells under steady-state conditions, the oxygen uptake rate OUR needs to be equal to the oxygen transfer rate OTR. The latter depends on mass transfer and the driving force on the gas-liquid surface, given as:

$$\underbrace{q_{O_2} \cdot X}_{OUR} = \underbrace{k_La \cdot \left(c^s_{O_2} - c_{O_2} \right)}_{OTR} \tag{20}$$

where q_{O_2}, X, c_{O_2} and $c^s_{O_2}$ represent the specific oxygen uptake rate, cell concentration, oxygen concentration and oxygen saturation concentration respectively. Typical specific oxygen demands reported for mammalian and insect cells range from about $1 \cdot 10^{-9}$ to $1 \cdot 10^{-8}$ mmol·cell^{-1}·day^{-1} (see also Tab. 3 for more details). Assuming oxygen solubility in cell culture media of 5 mg·L^{-1} and working at 30 % saturation, which are typical values in cell culture applications, the required k_La values for a cell density of $5 \cdot 10^6$ cells·mL^{-1} are between 1.1 and 36.8 h^{-1}, depending on the cell line. These values are already reached at an aeration rate of 0.1 vvm with a specific power input of about 140 W·m^{-3}, and with an even lower power input of about 10 W·m^{-3} at 0.2 vvm. In the CultiBag STR 50L a maximum k_La value of 35 h^{-1} was determined experimentally by Sartorius Stedim at an aeration rate of 0.1 vvm [Personal communication, Ute Noack, Sartorius Stedim Biotech, 2010], giving comparable results for the large scale bioreactor.

Cell line	q_{O2} [10^{-13} mol·cell^{-1}·h^{-1}]	k_La_{req} [h^{-1}]
C1a (hybridoma)	2.34	10.7
FS-4 (human diploid cells)	0.5	2.3
AB2-143.2(hybridoma)	1.9 – 4.0	8.7 – 18.3
167.4G5.3 (hybridoma)	0.23 – 0.87	1.1 – 4.0
NSO (myeloma)	2.19 – 4.06	10.0 – 18.6
MAK (hybridoma)	4.6	21.0
X-D (hybridoma)	2.3 – 4.2	10.5 – 19.2
DG44 (CHO)	2.0	9.1
CHO	5.0 – 8.04	22.9 – 36.8
HFN7.1 (hybridoma)	2.0	9.1

Table 3. Specific oxygen uptake rates of various cell lines adopted from Ruffieux et al. (1998) and Xiu et al. (1999) and required oxygen mass transfer coefficients at defined cell densities of $5 \cdot 10^6$ cells·mL^{-1} and oxygen concentrations of 5 mg·L^{-1} (see Eq. 20)

In spite of the numerous literature data in respect of oxygen mass transfer, no correlation was found for the particular stirrer configuration and operation conditions used in this study. Thus, a correlation was developed following an approach suggested by van't Riet (1979), where the k_La value is related to the specific power input and the superficial gas velocity (introduced gas per cross sectional area of the bioreactor):

$$k_La = C \cdot (P/V)^a \cdot \bar{u}_g{}^b \tag{21}$$

As shown in Fig. 10, very good agreements between the model and CFD-predicted k_La values are achieved for the two aeration rates investigated (with $R^2 = 0.98$). The coefficients C, a and b are found to be 6.51, 0.14 and 0.87 respectively (see Eq. 20). Hence, a rather high dependency of the k_La value on the superficial gas velocity (aeration rate) is evident and the specific power input is only of minor importance. This is in contrast to most correlations found in the literature, where the values for a and b are 0.5 ± 0.1 [Nienow (2006)]. Nevertheless, Van't Riet (1979) gives a wider range of reported values in the ranges of $0.4 < a < 1$ and $0 < b < 0.7$.

$$k_La = 6.51 \cdot (P/V)^{0.14} \cdot \bar{u}_g{}^{0.87} \tag{22}$$

The strong effect of the superficial gas velocity obtained in this study can be explained by the fact that the stirrer does not completely disperse the introduced gas at low agitation rates, and thus the aeration is comparable to a bubble column (see Fig. 9a). Similar results were recently found in our laboratory with other single-use stirred bioreactors (e.g. the Mobius® CellReady 3L bioreactor) [Kaiser et al. (2011)]. However, we would like to point

out that only twelve data points were used for the correlation in this first attempt and the results were only obtained by CFD simulations, which have to be validated by experimental data in further studies.

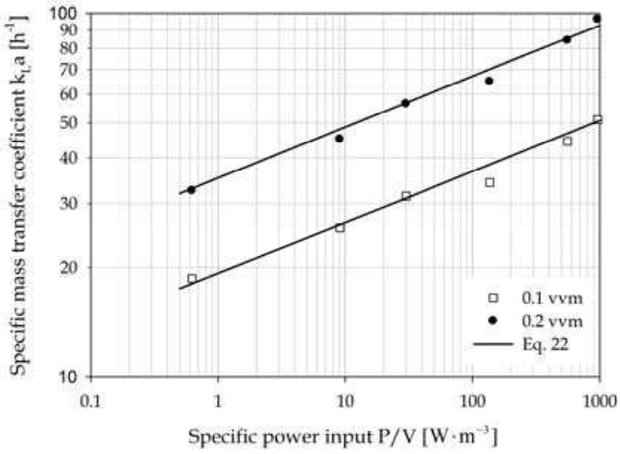

Fig. 10. CFD-predicted volume-averaged specific oxygen mass transfer coefficient k_La as a function of specific power input for the two aeration rates investigated. In addition to CFD-predicted data points, the function obtained by Eq. 22 is given

4.3 Mechanical stress

4.3.1 Mechanical stress caused by turbulence

Mechanical stress on cells is related to both turbulence and time-independent velocity-gradients (shear and normal gradients) [Jöbses et al. (1991); Oh et al. (1992); Chisti (2000); Fenge et al. (2003)]. A popular, but yet unproven, theory of cell damage due to turbulence suggests that the biological entity is damaged by eddies of a comparable size. Significantly smaller eddies have too little energy and larger eddies merely carry the cells convectively. Assuming local isotropic turbulence, the size of the smallest eddies is defined by the Kolmogorov length l_e (Eq. 23). Although Ranade & Joshi (1989) and Jaworski et al. (1991) state that turbulence in the impeller jet is anisotropic, theoretical considerations and experimental evidence have shown that the fine-scale structure of most anisotropic turbulent flows is actually almost isotropic locally [Hinze (1959)]. Thus, Kolmogorov's definition of eddy size would appear suitable for the complete fluid domain.

$$l_e = \left(\frac{\eta^3}{\rho^3 \cdot \varepsilon} \right)^{1/4} \tag{23}$$

In Fig. 11a, the dimensionless turbulent kinetic energy k/u_{tip}^2 is shown. As expected, and in agreement with Hockey & Nouri (1996), convection of turbulence by the mean flow in the impeller jet, where the highest turbulent energies are found, is evident. The axial profiles of the turbulence kinetic energy in impeller jets are found to qualitatively agree with data given by Kresta & Wood (1991), although the predicted values are, by a factor of 5, lower in our study (data not shown). Rather high turbulence is also located near the installations, but significantly lower values are found in the bulk between the impellers and near the liquid surface. Thus, it can be argued that the turbulence distribution is very heterogeneous. For

standard Rushton turbines, Höfken et al. (1996) found differences between maximum and mean turbulent dissipation rates by two orders of magnitude ($\varepsilon_{max} / \overline{\varepsilon} = 40...200$).

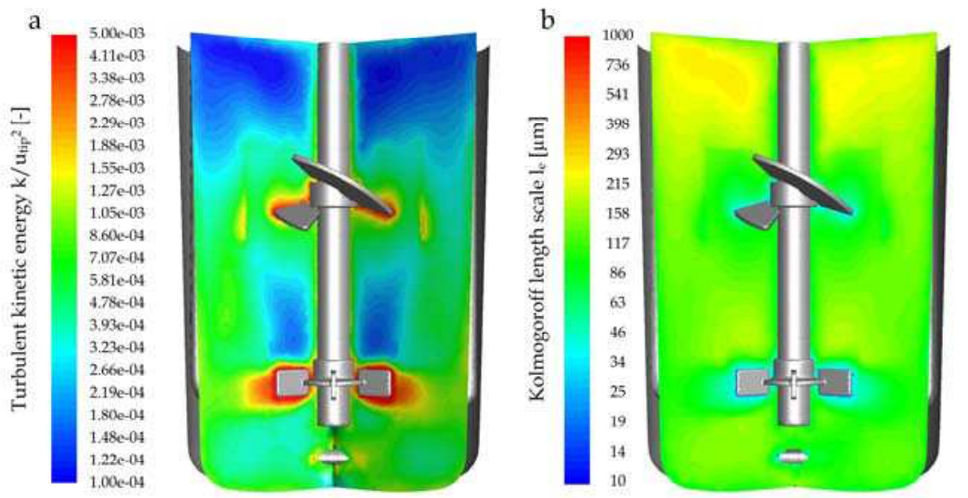

Fig. 11. Spatial distributions of the dimensionless turbulent kinetic energy k/u_{tip}^2 (a) and the Kolmogorov eddy size l_e (b) at P/V = 230 W·m^{-3} in the UniVessel® 2L single-use

As mentioned in Section 4.2.1, typical values for the specific power input are in the range of 10 to 250 W·m^{-3} [Nienow (2006)]. Calculating the Kolmogorov eddy size gives l_e = 45 µm for ε = (P/V) (see Eq. 23). If, as found by Höfken et al (1996) near the impeller of a Rushton turbine, $\varepsilon_{max} = 200 \cdot (P/V)$ is assumed, l_e decreases to about 12 µm. Since animal cells are of the order of 15-20 µm, the first cell damage would be expected at the maximum power input. In this study, the estimated Kolmogorov eddy size is lower than typical cell sizes above a specific power input of 230 W·m^{-3} (see Fig. 11b) in close proximity to the impellers and installations, which is in agreement with the literature data.

Zhang et al. (1993) investigated animal cell disruption in turbulent capillary flows and developed a model of cell-hydrodynamic interactions using cell mechanical properties determined by micromanipulation. Assuming that eddies with similar or smaller sizes than the cells cause local surface deformation, they proposed that cell disruption occurs when the cells' bursting membrane tension and bursting surface energy are exceeded. Good agreement between experiments and model predictions (with an underestimation of cell disruption by about 15%) were achieved [Zhang et al. (1993)].

Garcia-Briones et al. (1994) compared CFD-predicted energy dissipation rates with those in unaerated flow devices (capillaries and viscometers). They concluded that energy dissipation rates in the order of $5.81 \cdot 10^2$ W·m^{-3} did not damage cells significantly, but values of $\approx 2.25 \cdot 10^4$ W·m^{-3} caused considerable damage. Using Eq. 22, the latter value gives an eddy length scale of 14.5 µm for water-like media, which is comparable to the size of animal cells (≈15…20 µm).

The turbulence theory of cell damage is also supported by the observation that viscosifying additives reduce cell damage. Croughan et al. (1989) have associated cell death protection by serum with the turbulence-dampening effect of the additive. In contrast, observing an insect cell suspension with ten times higher viscosity to water (with $\eta \approx 10$ mPa·s and $\rho \approx 1000$ kg·m^{-3}), Tramper et al. (1996) found that cell death rapidly occurred from a specific power

input of $2.3 \cdot 10^{-3}$ W·kg^{-1}. Even if $\varepsilon_{max} / \bar{\varepsilon} \approx 200$ is assumed, this gives a minimum Kolmogorov length scale of l_e = 240 µm, which is considerably larger than an insect cell. Hence, it has been concluded that maximum shear stress is the more appropriate parameter for scale-up than the minimum eddy length scale [Tramper et al. (1996)].
However, bearing in mind the heterogeneous distribution of turbulence, it is important to take residence time distribution into account for the evaluation of cell damage (see Section 4.3.2 for further discussion). However, to the knowledge of the authors, such attempts have not yet been described for animal cells, unlike corresponding studies for blood cells in hemolysis experiments. Thus, the hemolysis level is often correlated with shear stress and residence time, as suggested, for example, by Giersiepen et al. (1990).

4.3.2 Mechanical stress caused by velocity gradients (shear stress)

In most CFD studies, the mechanical stress on cells is only related to the strain rate magnitude D, which is an invariant velocity gradient consisting of both shear and normal gradients. However, based on model experiments, various authors have shown that cells are differently affected by shear or normal gradients [e.g. Langer & Deppe (2000)]. It is therefore advantageous if each of them is quantified separately for the evaluation of cell damage. Recently, Wollny (2010) found that local shear and normal gradients (γ_{nt} and γ_{nn}) can be obtained from shear strain tensor using a coordinate system transformation, which results in Eqs. 24 and 25. Here, $\tilde{w}$ are velocities in the local co-ordinate systems defined by the co-ordinates $\tilde{x}, \tilde{y}$ and $\tilde{z}$, which are orientated along the fluid flow direction. Detailed descriptions of the mathematical derivation can be found elsewhere [Wollny (2010)].

$$\gamma_{nn} = \sqrt{2 \cdot \left(\frac{\partial \tilde{w}_x}{\partial \tilde{x}} \right)^2} \tag{24}$$

$$\gamma_{nt} = \sqrt{\left(\frac{\partial \tilde{w}_x}{\partial \tilde{y}} + \frac{\partial \tilde{w}_y}{\partial \tilde{x}} \right)^2 + \left(\frac{\partial \tilde{w}_x}{\partial \tilde{z}} + \frac{\partial \tilde{w}_z}{\partial \tilde{x}} \right)^2} \tag{25}$$

From the CFD-predicted flow fields, the local shear and normal gradients as well as the corresponding volume fractions were determined. Subsequently, the distribution was discretized into 250 bins (see Fig. 12a). It was found that the distribution follows a logarithmically normal function, which was confirmed by a chi-quadrate-test at a confidence level of 0.05 (data not shown).
From Fig. 12a it is evident that the highest volume fractions (of about 4.5 %) are found at very low velocity gradients. Depending on the impeller speed, the median value (velocity gradient with the highest volume fraction) is in the order of 1 – 30 s^{-1}. Interestingly, the median differs from the volume-averaged velocity gradient and the highest volume fraction is nearly independent of the stirrers' power input. This is in qualitative agreement with our previous findings for different single-use and conventional stirred bioreactors [Löffelholz et al. (2011)].
Furthermore, high velocity gradients (> 100 s^{-1}) have very small volume fractions below 0.5 % of the total liquid volume. Wollny (2010) found quantitatively comparable values for a baffled bioreactor equipped with a 3x24° pitched blade impeller or a standard Rushton

turbine operating at 100 W·m^{-3}. In this study, the impeller swept volume as described by Wollny (2010) is about 2 % of the total liquid volume for the stirrer configuration investigated. Thus, it can be argued that the regions of high 'shear' stress are positioned close to the impeller and that the cells are, if at all, mechanically stressed in only a small region of the bioreactor.

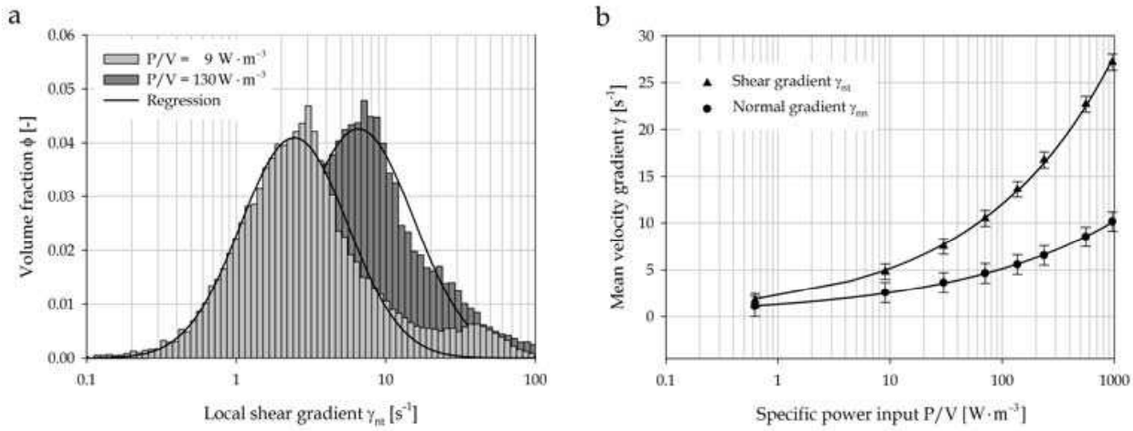

Fig. 12. Evaluation of mechanical damage to cells caused by local shear and normal gradients. Log-normal frequency distribution of local shear gradients (expressed by the volume fraction) for two agitation rates (a), and mean shear and normal velocity gradients as a function of the specific power input (b). Error bars represent simple standard deviation of the logarithmically normal distribution

In Fig. 12b, the mean velocity gradients obtained from the frequency distributions are given as a function of the specific power input. It is evident that the local shear gradients predominate compared with the normal gradients, which are suspected to cause higher cell damage [Langer & Deppe (2000)]. However, the magnitude of both mean and maximum velocity gradients is found to be significantly lower than the critical values (1 – 3 · 10^5 s^{-1}) causing substantial cell damage, as reported by Chisti (2001). Nevertheless, physiological effects, which do not necessarily require a physical breakage of the cells, were also observed at moderate levels of stress in the range of 0.5 – 5 N·m^{-2} (corresponding to 500 – 5000 s^{-1} in water-like culture broths) [Yim & Shamlou (2000)]. The maximum normal and shear gradients for the highest investigated power input (≈ 960 W·m^{-3}) reached values of up to 4800 and 6000 s^{-1} respectively. Consequently, based on the CFD results, no cell damage is expected in the small scale UniVessel® bioreactors at moderate agitation. A comparison of these results with the larger scale BIOSTAT® CultiBag STR will form part of further studies.

5. Conclusions

The first objective of this study was a comparison of the novel single-use UniVessel® cell culture bioreactor with its re-usable counterpart, developed by Sartorius Stedim Biotech. For this purpose, the fluid flow under non-aerated conditions was simulated using a RANS approach and the standard k-ε turbulence model. Almost identical flow patterns are achieved with only minor differences in fluid velocities and turbulence distributions, which can be attributed to small variations in the meshes and the positions of the installations such

as probes and harvest tubes. The CFD simulations reveal a rather complex flow pattern, in which the radial pumping Rushton turbine induced two flow loops per half-vessel and the segment blade impeller shows a typical axial flow in down-pumping mode.

Predicted fluid velocities as well as flow numbers show good qualitative and quantitative agreement with literature data. Based on these results, it can be argued that the differences in geometry between the two small scale bioreactors have no influence on the overall fluid flow. From the fluid flow perspective, the UniVessel® 2L single-use is identical to its counterpart made of glass and thus no differences in cell cultivations are expected. This hypothesis clearly needs to be verified in cultivation experiments, which will be carried out in our laboratory in the near future.

In a second part, key engineering parameters, such as power input, mixing capacity and oxygen mass transfer, for the UniVessel® 2L single-use are presented for the first time and compared with data on its conventional counterpart as well as with those on the BIOSTAT® CultiBag STR 50L. The power numbers Ne of the two small scale systems are identical (with a value of 3.33) and somewhat lower in the CultiBag STR 50L (Ne = 3.14) at the same stirrer configuration (RT and SBI). It is shown that unreasonably high specific power inputs for cell culture applications are obtained in the UniVessel® bioreactors, if the maximum tip speed of 1.8 $m \cdot s^{-1}$ is used as a scale-up/down parameter for the CultiBag STR 50L. Thus, it can be concluded that (maximum) specific power input P/V is a more appropriate constraint for scale-up than tip speed when viewed from the perspective of adequate mixing and shear sensitivity of the cells, which is in agreement with the literature data. Furthermore, correlations for the mixing time are provided which are independent of the bioreactor scale, as suggested by Nienow (1997), and can thus be used in scale-up/down studies.

From multi-phase simulations using an Euler-Euler approach, gas phase distribution and oxygen mass transfer were modelled for various agitation and aeration rates. In this first attempt, a constant bubble size of 1 mm, as obtained using photography at the BIOSTAT® B plus is assumed. It is well-known that bubble size depends on media properties, such as viscosity, salt content etc., and is usually non-uniform. In addition, bubble size distribution depends on aeration (e.g. the sparger design) and the agitation system (e.g. impeller type), and is further influenced by bubble break-up and coalescence. In the last two decades, bubble size distributions have been increasingly modelled using population balance models (PBM) [e.g. Kerdouss et al. (2008); Dhanasekharan et al. (2005)]. Nevertheless, computation using PBMs becomes more complex and time-consuming due to the additional transport equations for bubble size distribution. Hence, this approach is not adopted for the first engineering characterization of the UniVessel®, but will be used in further studies in the near future. Based on the results obtained so far, it can be concluded that the oxygen transfer capacity of the UniVessel® 2L single-use has no limitations for medium cell densities achieved at gentle agitation and aeration. In addition to the results presented, the fluid flow in the small scale UniVessel® equipped with two segment blade impellers will be investigated in further studies, because Sartorius Stedim decided to provide the UniVessel® single-use with this stirrer configuration mainly due to the broad acceptance by the costumers.

In a third part, two approaches for the evaluation of mechanical stress on cells are presented. The first, which is based on the Kolmogorov turbulence theory, indicates that cell damage could occur above specific power inputs of 230 $W \cdot m^{-3}$. This value is also given as the upper limit of typical power inputs by Nienow (2006). However, it is shown that the

turbulence distribution inside the bioreactor is very heterogeneous. Hence, volume-weighted distributions of velocity gradients are predicted in the second approach. These velocity gradients are additionally subdivided into local shear and normal gradients, as suggested by Wollny (2010), which may allow a more detailed evaluation of cell damage mechanisms. Compared with turbulence, velocity gradients indicate lower cell stress potential. Although no cell damage is expected under typical operation conditions, it is difficult to draw general conclusions since biological effects depend on various factors, such as the cell line used, cell characteristics, culture media, additives and so on. Nevertheless, the results obtained indicate that Sartorius Stedim's novel UniVessel® 2L single-use is a viable alternative to conventional stirred cell culture bioreactors at bench scale.

6. Acknowledgment

The results presented are part of PhD theses. The authors are grateful to Dipl.-Ing. Ute Noack, Dr. Alexander Tappe, Dr. Gerhard Greller, Dr. Bhaskar Bandarapu, Dr. Thorsten Peuker, Dipl.-Ing. Lars Böttcher, Martin Saballus and Alexander Halt from Sartorius Stedim Biotech for providing details about the geometries of the bioreactors investigated and the experimental results of the BIOSTAT® CultiBag STR 50L as well as for their participation in helpful discussions.

7. References

Alcamo, R.; Micale, G.; Grisafi, F.; Brucato, A. & Ciofalo, M. (2005). Large-eddy simulation of turbulent flow in an unbaffled stirred tank driven by a Rushton turbine. *Chemical Engineering Science*, Vol. 60, pp. 2303-2316

Arathoon, W. & Birch, J. (1986). Large scale cell culture in biotechnology. *Science,* Vol. 232, pp. 1390-1395

Chalmers, J. J. (1994). Cells and bubbles in sparged bioreactors. *Cytotechnology,* Vol. 15, pp. 311-320

Chisti, Y. (1993). Animal cell culture in stirred bioreactors: Observations on scale-up. *Bioprocess Engineering,* Vol. 9, pp. 191-196

Chisti, Y. (2000). Animal-cell damage in sparged bioreactors. *Trends in Biotechnology,* Vol. 18, pp. 420-432

Chisti, Y. (2001). Hydrodynamic damage to animal cells. *Critical Reviews in Biotechnology,* Vol. 21, pp. 67-110

Croughan, M. S.; Sayre, E. S. & Wang, D. I. (1989). Viscous reduction of turbulent damage in animal cell culture. *Biotechnology and Bioengineering, Vol. 33*, pp. 862-872

De Wilde, D.; Noack, U.; Kahlert, W.; Barbaroux, M. & Greller, G. (2009). Bridging the gap from reusable to single-use manufacturing with stirred, single-use bioreactors. *BioProcess International,* Vol. 7, pp. 36-41

Delafosse, A.; Line, A.; Morchain, J. & Guiraud, P. (2008). LES and URANS simulations of hydrodynamics in mixing tank: comparison to PIV experiments. *Chemical Engineering Research and Design,* Vol. 86, pp. 1322-1330

Dhanasekharan, K. M.; Sanyal, J.; Jain, A. & Haidari, A. (2005). A generalized approach to model oxygen transfer in bioreactors using population balances and computational fluid dynamics. *Chemical Engineering Science*, Vol. 60, pp. 213-218

Eibl, R.; Kaiser, S.; Lombriser, R. & Eibl, D. (2010). Disposable bioreactors: the current state-of-the-art and recommended applications in biotechnology. *Applied Microbiology Biotechnology*, Vol. 86, pp. 41-49

Eibl, R.; Löffelholz, C. & Eibl, D. (2011). Single-use bioreactors - an overview, In: *Single-use Technology in Biopharmaceutical Manufacture*, *R.* Eibl & D. Eibl, (Eds.), 34-51, John Wiley & Sons, New Jersey, USA

Fenge, C.; Klein, C.; Heuer, C.; Siegel, U. & Fraune, E. (1993). Agitation, aeration and perfusion modules for cell culture bioreactors. *Cytotechnology* , Vol. 11, pp. 233-244

Fluent 6.3 user's guide (2006), Centerra Resource Park, 10 Cavendish Court, Lebanon, USA: Fluent Inc., Available from http://my.fit.edu/itresources/manuals/fluent6.3/help/pdf/ug/flug.pdf

Garcia-Briones, M. & Chalmers, J. J. (1994). Flow parameters associated with hydrodynamic cell injury. *Biotechnology and Bioengineering,* Vol. 44, pp. 1089-1098

Giersiepen, M.; Wurzinger, L.; Optz, R. & Reul, H. (1990). Estimation of shear stress-related blood damage in heart valve protheses - in vitro comparison of 25 aortic valves. *International Journal of Artificial Organs*, Vol. 13, pp. 300-306

Gimbun, J.; Rielly, C. & Nagy, Z. (2009). Modelling of mass transfer in gas–liquid stirred tanks agitated by rushton turbine and CD-6 impeller: A scale-up study. *Chemical Engineering Research and Design,* Vol. 87, pp. 437-451

Handa, A.; Emery, A. & Spier, R. (1987). On the evaluation of gas-liquid interfacial effects on hybridoma viability in bubble column bioreactors. *Developments in Biological Standardization,* Vol. 66, pp. 241-253

Henzler, H.-J. & Kauling, D. J. (1993). Oxygenation of cell cultures. *Bioprocess and Biosystems Engineering*, Vol. 9, pp. 61-75

Hinze, J.O. (1959). *Turbulence*. McGraw-Hill, New York.

Hockey, R. M. & Nouri, J. (1996). Turbulent flow in a baffled vessel stirred by a 60° pitched blade impeller. *Chemical Engineering Science,* Vol. 51, pp. 4405-4421

Höfken, M.; Schäfer, M. & Durst, F. (1996). Detaillierte Untersuchung des Strömungsfeldes innerhalb eines Sechs-Blatt-Scheibenrührers. *Chemie lngenieur Technik,* Vol. 68, pp. 803-809

Ishii, M. & Zuber, N. (1979). Drag coefficient and relative velocity in bubbly, droplet or particulate flows. *AIChE Journal,* Vol. 25, pp. 843-855

Jahoda, M.; Mostek, M.; Kukuková, A. & Machon, V. (2007). CFD modelling of liquid homogenization in stirred tanks with one and two impellers using large eddy simulation. *Chemical Engineering Research and Design,* Vol. 85, pp. 616-625

Jaworski, Z.; Nienow, A. W.; Koutsakos, E.; Dyster, K. & Bujalski, W. (1991). An LDA study of turbulent flow in a baffled vessel agitated by a pitched blade turbine. *Chemical Engineering Research and Design,* Vol. 69, pp. 313-320

Jöbses, I.; Martens, D. & Tramper, J. (1991). Lethal events during gas sparging in animal cell culture. *Biotechnology and Bioengineering,* Vol. 37, pp. 484-490

Kaiser, S.C. (2009). Theoretische und experimentelle Untersuchungen zur Bestimmung der Mischzeit und des Sauerstoffeintrages in Bioreaktoren. Master Thesis. Hochschule Anhalt (FH), Köthen..

Kaiser, S. C.; Eibl, R. & Eibl, D. (2011). Engineering characteristics of a single-use stirred bioreactor at bench-scale: The Mobius CellReady 3L bioreactor as a case study, *Engineering Life Sciences,* in submission.

Kerdouss, F.; Bannari, A.; Proulx, P.; Bannari, R.; Skrga, M. & Labrecque, Y. (2008). Two-phase mass transfer coefficient prediction in stirred vessel with a CFD model. *Computers and Chemical Engineering,* Vol. 32, pp. 1943-1955

Kioukia, N.; Nienow, A. W.; Al-Rubeai, M. & Emery, A. N. (1996). Influence of agitation and sparging on the growth rate and infection of insect cells in bioreactors and a comparison with hybridoma culture. *Biotechnol. Prog.,* Vol. 12, pp. 779-785

Krampe, B. & Al-Rubeai, M. (2010). Cell death in mammalian cell culture: molecular mechanisms and cell line engineering strategies. *Cytotechnology,* Vol. 62, pp. 175-188

Kraume, M. (2003). *Mischen und Rühren. Grundlagen und moderne Verfahren*. Wiley-VCH

Kresta, S. & Wood, P. (1991). Prediction of the three-dimensional turbulent flow in stirred tanks. *AIChE Journal,* Vol. 37, pp. 448-460

Langer, G. & Deppe, A.(2000). Zum Verständnis der hydrodynamischen Beanspruchung von Partikeln in turbulenten Rührerströmungen. *Chemie Ingenieur Technik,* Vol. 72, pp. 31-41

Langheinrich, C.; Nienow, A. W.; Eddleston, T.; Stevenson, N. C.; Emery, A. N.; Clayton, T. M. & Slater, N. K. H. (2002). Oxygen transfer in stirred bioreactors under animal cell culture conditions. *Food and Bioproducts Processing,* Vol. 80, pp. 39-44

Letellier, B.; Xuereb, C.; Swaels, P.; Hobbes, P. & Bertrand, J. (2002). Scale-up in laminar and transient regimes of a multi-stage stirrer, a CFD approach. *Chemical Engineering Science,* Vol. 57, pp. 4617 - 4632

Liepe, F.; Sperling, R. & Jembere, S. (1998). *Rührwerke - Theoretische Grundlagen, Auslegung und Bewertung*. Eigenverlag FH Anhalt, Köthen

Löffelholz, C.; Kaiser, S.; Werner, S. & Eibl, D. (2011). CFD as a tool to characterize single-use bioreactors, In: *Single-use Technology in Biopharmaceutical Manufacture, R.* Eibl & D. Eibl, (Eds.), 34-51, John Wiley & Sons, New Jersey, USA

Meneses-Acosta, A.; Mendonca, R. Z.; Merchant, H.; Covarrubias, L. & Ramírez, O. T. (2001). Comparative characterization of cell death between Sf9 insect cells and hybridoma cultures. *Biotechnology and Bioengineering,* Vol. 72, pp. 441-457

Min, J. & Gao, Z. (2006). Large eddy simulation of mixing time in a stirred tank. *Chinese Journal Chemical Engineering,* Vol. 14, pp. 1-7

Montante, G.; Lee, K.; Brucato, A. & Yianneskis, M. (2001). Numerical simulations of the dependency of flow pattern on impeller clearance in stirred vessels. *Chemical Engineering Science,* Vol. 56, pp. 3751-3770

Nienow, A. W. (1997). On impeller circulation and mixing effectiveness in the turbulent flow regime. *Chemical Engineering Science,* Vol. 52, pp. 2557-2565

Nienow, A. W. (2006). Reactor engineering in large scale animal cell culture. *Cytotechnology,* Vol. 50, pp. 9-33

Noack, U.; De Wilde, D.; Verhoeye, F.; Balbirnie, E.; Kahlert, W.; Adams, T.; Greller, G. & Reif, O. (2011). Single-use stirred tank reactor BIOSTAT CultiBag STR: Characterization and applications, In: *Single-use Technology in Biopharmaceutical Manufacture, R.* Eibl & D. Eibl, (Eds.), 34-51, John Wiley & Sons, New Jersey, USA

Oh, S.; Nienow, A.; AI-Rubeai, M. & Emery, A. (1992). Further studies of the culture of mouse hybridomas in an agitated bioreactor with and without continuous sparging. *Journal of Biotechnology,* Vol. 22, pp. 245-270

Ozturk, S. S. (1996). Engineering challenges in high density cell culture systems. *Cytotechnology,* Vol. 22, pp. 3-16

Paschedag, A. R.; Kassera, V. & Sperling, R. (2007). Aktuelle Entwicklungen in der CFD für gerührte Systeme. *Chemie Ingenieur Technik,* Vol. 79, pp. 983-999

Patwardhan, A. W. & Joshi, J. B. (1999). Relation between flow pattern and blending in stirred tanks. *Industrial& Engineering Chemistry Research,* Vol. 38, pp. 3131-3143

Ranade, V. V. & Joshi, J. B. (1989). Flow generated by pitched blade turbines I: measurements using laser Doppler anemometer. *Chemical Engineering Communications,* Vol. 81, pp. 197-224

Revstedt, J.; Fuchs, L. & Trägardh, C. (1998). Large eddy simulations of the turbulent flow in a stirred reactor. *Chemical Engineering Science,* Vol. 53, pp. 4041-4053

Ruffieux, P.-A.; von Stockar, U. & Marison, I. W. (1998). Measurement of volumetric (OUR) and determination of specific (qO2) oxygen uptake rates in animal cell cultures. *Journal of Biotechnology,* Vol. 63, pp. 85-95

Tramper, J.; Vlak, J. & de Gooijer, C. (1996). Scale up aspects of sparged insect-cell bioreactors. *Cytotechnology,* Vol. 20, pp. 221-229

Storhas, W. (2003). *Bioverfahrensentwicklung*. Wiley-VCH, Weinheim.

Van't Riet, K. (1979). Review of measuring methods and results in nonviscous gas-liquid mass transfer in stirred vessels. *Industrial & Engineering Chemistry Process Design and Development*, Vol. 18, pp. 1979 357

Varley, J. & Birch, J. (1999). Reactor design for large scale suspension animal cell culture. *Cytotechnology,* Vol. 29, pp. 177-205

Venkat, R. V. & Chalmers, J. J. (1996). Characterization of agitation environments in 250 ml spinner vessel, 3 L, and 20 L reactor vessels used for animal cell microcarrier culture. *Cytotechnology,* Vol. 22, pp. 95-102

Vrabel, P.; van der Lans, R. G. J. M.; Luyben, K. C. A. M.; Boon, L. & Nienow, A. W. (2000). Mixing in large-scale vessels stirred with multiple radial or radial and axial up-pumping impellers: modelling and measurements. *Chemical Engineering Science,* Vol. 55, pp. 5881-5896

Weyand, B.; Israelowitz, M.; von Schroeder, H. & Vogt, P. (2009). Fluid dynamics in bioreactor design: considerations for the theoretical and practical approach, In: *Bioreactor Systems for Tissue Engineering*, C. Kasper, M. van Griensven & R. Pörtner (Eds.), 251-268

Wollny, S. (2010). Experimentelle und numerische Untersuchungen zur Partikelbean-spruchung in gerührten (Bio-)Reaktoren. PhD thesis. Technische Universität Berlin, Deutschland

Xiu, Z.-L.; Deckwer, W.-D. & Zeng, A.-P. (1999). Estimation of rates of oxygen uptake and carbon dioxide evolution of animal cell culture using material and energy balances. *Cytotechnology,* Vol. 29, pp. 159-166

Yianneskis, M.; Popiolek, Z. & Whitelaw, J. (1987). An experimental study of the steady and unsteady flow characteristics of stirred reactors. *Journal of Fluid Mechanics,* Vol. 175, pp. 537-555

Yim, S. S. & Shamlou, P. A. (2000). The engineering effects of fluids flow on freely suspended biological macro-materials and macromolecules, In: *Influence of Stress on Cell Growth and Product Formation*, K. Schügerl & G. Kretzmer, (Eds.), 83-122, Springer

Zhang, Z.; Al-Rubeai, M. & Thomas, C. R. (1993). Estimation of disruption of animal cells by turbulent capillary flow. *Biotechnology and Bioengineering*, Vol. 42, pp. 987-993

Zhu, H.; Nienow, A. W.; Bujalski, W. & Simmons, M. J. (2009). Mixing studies in a model aerated bioreactor equipped with an up- or a down-pumping 'Elephant Ear' agitator: Power, hold-up and aerated flow field measurements. *Chemical Engineering Research and Design,* Vol. 87, pp. 307-317

Zlokarnik, M.(1999). *Rührtechnik - Theorie und Praxis*. Springer, Berlin, Heidelberg, New York

Zlokarnik, M. (2006). *Scale-Up in Chemical Engineering (second, completely revised and extended edition)*. Wiley-VCH, Weinheim

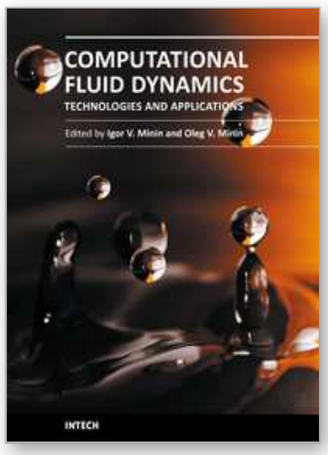

Computational Fluid Dynamics Technologies and Applications
Edited by Prof. Igor Minin

ISBN 978-953-307-169-5
Hard cover, 396 pages
Publisher InTech
Published online 05, July, 2011
Published in print edition July, 2011

This book is planned to publish with an objective to provide a state-of-art reference book in the area of computational fluid dynamics for CFD engineers, scientists, applied physicists and post-graduate students. Also the aim of the book is the continuous and timely dissemination of new and innovative CFD research and developments. This reference book is a collection of 14 chapters characterized in 4 parts: modern principles of CFD, CFD in physics, industrial and in castle. This book provides a comprehensive overview of the computational experiment technology, numerical simulation of the hydrodynamics and heat transfer processes in a two dimensional gas, application of lattice Boltzmann method in heat transfer and fluid flow, etc. Several interesting applications area are also discusses in the book like underwater vehicle propeller, the flow behavior in gas-cooled nuclear reactors, simulation odour dispersion around windbreaks and so on.

INTECH
open science | open minds

InTech Europe
University Campus STeP Ri
Slavka Krautzeka 83/A
51000 Rijeka, Croatia
Phone: +385 (51) 770 447
Fax: +385 (51) 686 166
www.intechopen.com

InTech China
Unit 405, Office Block, Hotel Equatorial Shanghai
No.65, Yan An Road (West), Shanghai, 200040, China
中国上海市延安西路65号上海国际贵都大饭店办公楼405单元
Phone: +86-21-62489820
Fax: +86-21-62489821

IntechOpen